Analyzing diffraction gratings by a boundary integral equation Neumann-to-Dirichlet map method

Yumao Wu[1,2,3] and Ya Yan Lu[3]

[1]*Joint Advanced Research Center of University of Science and Technology of China and City University of Hong Kong, Suzhou, Jiangsu, China*

[2]*Department of Mathematics, University of Science and Technology of China, Hefei, Anhui, China*

[3]*Department of Mathematics, City University of Hong Kong, Kowloon, Hong Kong*

For analyzing diffraction gratings, a new method is developed based on dividing one period of the grating into homogeneous sub-domains and computing the Neumann-to-Dirichlet (NtD) maps for these sub-domains by boundary integral equations. For a sub-domain, the NtD operator maps the normal derivative of the wave field to the wave field on its boundary. The integral operators used in this method are simple to approximate, since they involve only the standard Green's function of the Helmholtz equation in homogeneous media. The method retains the advantages of existing boundary integral equation methods for diffraction gratings, but avoids the quasi-periodic Green's functions that are expensive to evaluate.

OCIS codes: 050.1755,050.1960,000.4430

1. Introduction

Diffraction gratings [1–3] are important in many practical applications. Numerical methods are essential in the design, analysis and optimization of grating structures. Over the last several decades, many rigorous numerical or semi-analytic methods have been developed. Existing methods for diffraction gratings include the analytic modal method [4–6], the Fourier modal method (FMM) [7–10], the differential method [11, 12], the integral equation method [13–19], the coordinate transformation method (C method) [20–22], the finite element method (FEM) [23], etc. The analytic modal method and FMM are suitable for diffraction gratings involving uniform layers, but they are not as efficient and may have convergence problems when a general grating with sloping interfaces must be approximated by a multilayered

one [24]. The boundary integral equation (BIE) method is suitable if the grating structure involves a small number of interfaces and the refractive index is piecewise constant, but it is somewhat complicated to implement, since the integral operators are related to the quasi-periodic Green's function which requires sophisticated lattice sums techniques to evaluate. The FEM is very general, but it gives rise to large, complex and indefinite linear systems that are expensive to solve.

Recently, we developed a Dirichlet-to-Neumann (DtN) map method for scattering problems of periodic arrays of cylinders (as finite photonic crystals) [25–28]. Most existing methods for diffraction gratings are applicable to the problems studied in these works, but special methods taking advantage of the geometry features are often more efficient. Both the multipole method [29, 30] and the DtN map method are efficient for analyzing arrays of circular cylinders due to their use of cylindrical waves. However, the multipole method requires lattice sums to handle the infinite number of cylinders in each array. The DtN map method can avoid lattice sums, since it only uses the cylindrical waves in each unit cell to construct matrix approximations to an operator defined on the boundary of the unit cell. The involved operator is the DtN map that relates the wave field components to their normal derivatives on the cell boundary. In this paper, we develop a new method for general diffraction grating problems. The method divides one period of the grating into sub-domains with constant refractive indices and uses a boundary integral equation to find the Neumann-to-Dirichlet (NtD) map (the inverse of the DtN map) for each sub-domain. Unlike the existing integral equation methods, the integral operators in our method are simple to approximate, since they are related to the standard Green's function of the Helmholtz equation in an infinite homogeneous medium.

2. Problem formulation

We consider diffraction gratings which are invariant in the z direction and periodic in the x direction with a period L, where $\{x, y, z\}$ is a Cartesian coordinate system. A typical example is shown in Fig. 1. For waves propagating in the xy-plane, the transverse electric (TE) and transverse magnetic (TM) polarizations can be studied separately. The governing equations are

$$\rho\frac{\partial}{\partial x}\left(\frac{1}{\rho}\frac{\partial u}{\partial x}\right)+\rho\frac{\partial}{\partial y}\left(\frac{1}{\rho}\frac{\partial u}{\partial y}\right)+k_0^2\varepsilon u=0, \tag{1}$$

where $\varepsilon=\varepsilon(x,y)$ is the dielectric function, $k_0=\omega/c$ is the free space wavenumber, ω is the angular frequency and c is the speed of light in vacuum. For the TE case, u is the z-component of the electric field and $\rho=1$; for the TM case, u is the z component of the magnetic field and $\rho=\varepsilon$. The periodic structure is restricted to the region given by $0<y<D$ for some positive D. In the top ($y>D$) and bottom ($y<0$) regions, the medium is isotropic and

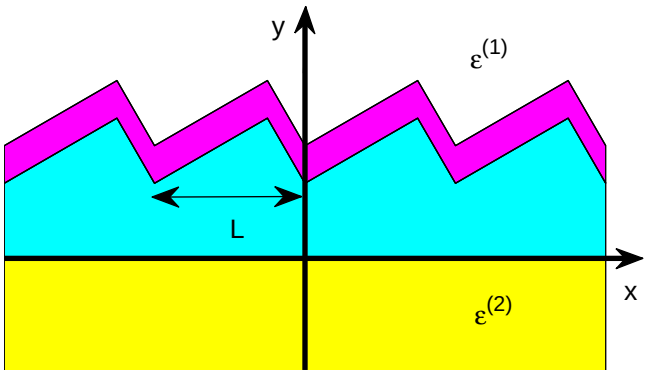

Fig. 1. A typical diffraction grating.

homogeneous. We have $\varepsilon = \varepsilon^{(1)}$ and $\varepsilon = \varepsilon^{(2)}$ for $y > D$ and $y < 0$ respectively, where $\varepsilon^{(1)}$ and $\varepsilon^{(2)}$ are constants.

For a plane incident wave given in the top region, i.e.,

$$u^{(i)}(x,y) = e^{i(\alpha_0 x - \beta_0^{(1)} y)}, \quad y > D, \tag{2}$$

where $\alpha_0^2 + [\beta_0^{(1)}]^2 = k_0^2 \varepsilon^{(1)}$ and $\beta_0^{(1)} > 0$, our objective is to determine the reflected and transmitted waves which are expanded in plane waves as

$$u^{(r)}(x,y) = \sum_{j=-\infty}^{\infty} R_j e^{i(\alpha_j x + \beta_j^{(1)} y)}, \quad y > D, \tag{3}$$

$$u^{(t)}(x,y) = \sum_{j=-\infty}^{\infty} T_j e^{i(\alpha_j x - \beta_j^{(2)} y)}, \quad y < 0, \tag{4}$$

where R_j and T_j are the reflection and transmission amplitudes, and

$$\alpha_j = \alpha_0 + \frac{2j\pi}{L}, \quad \beta_j^{(s)} = \sqrt{k_0^2 \varepsilon^{(s)} - \alpha_j^2}, \quad s = 1, 2. \tag{5}$$

Mathematically, the problem can be formulated in a two-dimensional (2D) rectangular domain $\Sigma = \{(x,y) \,|\, 0 < x < L,\, 0 < y < D\}$ [31]. Due to the periodicity of the structure and the x-dependence of the incident wave, the solution is quasi-periodic:

$$u(L,y) = \gamma\, u(0,y), \quad \frac{\partial u}{\partial x}(L^+, y) = \gamma\, \frac{\partial u}{\partial x}(0^+, y), \tag{6}$$

where $\gamma = e^{i\alpha_0 L}$. For the TM polarization, the normal derivative of u is not continuous on a material interface. To include the possibility of a vertical interface at $x = 0$ (and $x = L$), we

choose to use the right limit of $\partial_x u$ to impose the quasi-periodic condition above. Meanwhile, let $\mathcal{B}^{(1)}$ and $\mathcal{B}^{(2)}$ be linear operators acting on quasi-periodic functions of x, satisfying

$$\mathcal{B}^{(s)}\, e^{i\alpha_j x} = \beta_j^{(s)} e^{i\alpha_j x}, \quad j = 0, \pm 1, \pm 2, ... \tag{7}$$

for $s = 1$ and 2, then the top and bottom boundary conditions are [25, 31]:

$$\frac{\partial u}{\partial y} = -i\mathcal{B}^{(2)} u, \quad y = 0^-, \tag{8}$$

$$\frac{\partial u}{\partial y} = i\mathcal{B}^{(1)} u - 2i\beta_0 e^{i\alpha_0 x}, \quad y = D^+. \tag{9}$$

Notice that the boundary conditions are posed at $y = 0^-$ and $y = D^+$ using one-sided limits, since $\partial_y u$ (for the TM polarization) may be discontinuous if $y = 0$ and/or $y = D$ coincide with a material interface. In practice, the operators $\mathcal{B}^{(1)}$ and $\mathcal{B}^{(2)}$ are approximated by matrices.

3. Operator marching scheme

The operator marching (OM) method has its origin in an early work on acoustic waveguides [32]. Following the recent work [25, 27] for finite photonic crystals (PhCs), we divide the rectangular domain Σ into a number of sub-domains Ω_1, Ω_2, ..., Ω_m, and assume that they are separated and bounded by curves Γ_0, Γ_1, ..., Γ_m and two vertical lines at $x = 0$ and $x = L$. In particular, Γ_0 and Γ_m correspond to the line segments at $y = 0$ and $y = D$, respectively. For the diffraction grating shown in Fig. 1, the domain Σ and the sub-domains are depicted

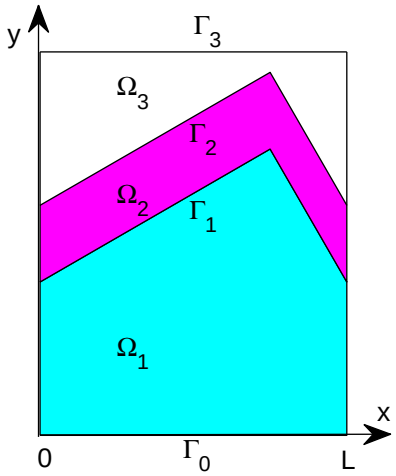

Fig. 2. Rectangular domain Σ for one period of a diffraction grating.

in Fig. 2. Notice that the sub-domains always have corners even when the grating profile is

smooth. On Γ_j, we define operators $\mathcal{Q}_j^{\pm}$ and $\mathcal{Y}_j$ satisfying

$$\mathcal{Q}_j^{\pm}\, u|_{\Gamma_j} = \left.\frac{\partial u}{\partial \nu}\right|_{\Gamma_j^{\pm}}, \quad \mathcal{Y}_j\, u|_{\Gamma_j} = u|_{\Gamma_0}, \tag{10}$$

where ν is an upward unit normal vector of Γ_j and u is an arbitrary solution satisfying the Helmholtz equation (1), the quasi-periodic condition (6) and the boundary condition (8).

From boundary condition (8) and the definition of $\mathcal{Y}_0$, we can initialize $\mathcal{Q}_0^-$ and $\mathcal{Y}_0$ by

$$\mathcal{Q}_0^- = -i\mathcal{B}^{(2)}, \quad \mathcal{Y}_0 = \mathcal{I}, \tag{11}$$

where $\mathcal{I}$ is the identity operator. The continuity of $\rho^{-1}\partial_\nu u$ gives

$$\frac{1}{\rho|_{\Gamma_j^+}}\mathcal{Q}_j^+ = \frac{1}{\rho|_{\Gamma_j^-}}\mathcal{Q}_j^-. \tag{12}$$

If $\mathcal{Q}_m^+$ and $\mathcal{Y}_m$ are calculated, we can solve u at $y = D$ from boundary condition (9), i.e.,

$$[\mathcal{Q}_m^+ - i\mathcal{B}^{(1)}]\, u(x, D) = -2i\beta_0 e^{i\alpha_0 x}. \tag{13}$$

After that, we can find the transmitted wave from

$$u(x, 0) = \mathcal{Y}_m u(x, D) \tag{14}$$

and find the reflected wave by subtracting the incident wave from the total field.

Therefore, the key step is to calculate $\mathcal{Q}_j^-$ and $\mathcal{Y}_j$ from $\mathcal{Q}_{j-1}^+$ and $\mathcal{Y}_{j-1}$. In previous work on arrays of cylinders (as finite PhCs) [25, 27], this step is carried out by first calculating the Dirichlet-to-Neumann (DtN) map of the sub-domain Ω_j. The DtN map of Ω_j is the operator Λ_j satisfying

$$\Lambda_j\, u = \frac{\partial u^{(in)}}{\partial \nu} \quad \text{on} \quad \partial\Omega_j \tag{15}$$

where u is any solution of Eq. (1), $\partial\Omega_j$ is the whole boundary of Ω_j, ν is a unit normal vector of $\partial\Omega_j$ and the subscript (in) signifies that the normal derivative is the limit towards $\partial\Omega_j$ from the interior of Ω_j. For PhCs, Ω_j is usually a unit cell with a simple square or hexagon shape, and the DtN map Λ_j can be constructed from special solutions, such as the cylindrical harmonics. For diffraction gratings, we choose Ω_j to be a sub-domain with a homogeneous medium. Since the shape of Ω_j is quite irregular, the method for constructing Λ_j using special solutions is no longer reliable, because the process may involve the inversion of near singular matrices. In Section 4, we use boundary integral equations to approximate the inverse of Λ_j, i.e., the Neumann-to-Dirichlet (NtD) map. The NtD map $\mathcal{V}_j = \Lambda_j^{-1}$ is easier to approximate and it still allows us to march the operators from Γ_{j-1} to Γ_j.

Let us write down the NtD map $\mathcal{V}_j$ in more details as

$$\mathcal{V}_j \begin{bmatrix} \partial_\nu u_{j-1}^+ \\ \partial_x v_j^+ \\ \partial_x w_j^- \\ \partial_\nu u_j^- \end{bmatrix} = \begin{bmatrix} \mathcal{V}_{11}^{(j)} & \mathcal{V}_{12}^{(j)} & \mathcal{V}_{13}^{(j)} & \mathcal{V}_{14}^{(j)} \\ \mathcal{V}_{21}^{(j)} & \mathcal{V}_{22}^{(j)} & \mathcal{V}_{23}^{(j)} & \mathcal{V}_{24}^{(j)} \\ \mathcal{V}_{31}^{(j)} & \mathcal{V}_{32}^{(j)} & \mathcal{V}_{33}^{(j)} & \mathcal{V}_{34}^{(j)} \\ \mathcal{V}_{41}^{(j)} & \mathcal{V}_{42}^{(j)} & \mathcal{V}_{43}^{(j)} & \mathcal{V}_{44}^{(j)} \end{bmatrix} \begin{bmatrix} \partial_\nu u_{j-1}^+ \\ \partial_x v_j^+ \\ \partial_x w_j^- \\ \partial_\nu u_j^- \end{bmatrix} = \begin{bmatrix} u_{j-1} \\ v_j \\ w_j \\ u_j \end{bmatrix} \tag{16}$$

where $v_j = u|_{x=0}$, $w_j = u|_{x=L}$, $u_{j-1} = u|_{\Gamma_{j-1}}$, $u_j = u|_{\Gamma_j}$, and Λ_j^{-1} is partitioned as 4×4 blocks. Similar to the case for Λ_j given in [25], if we insert the quasi-periodic condition (6) into (16), we can eliminate v_j, w_j and their x derivatives. This leads to the reduced NtD map $\mathcal{N}_j$ satisfying

$$\mathcal{N}_j \begin{bmatrix} \partial_\nu u_{j-1}^+ \\ \partial_\nu u_j^- \end{bmatrix} = \begin{bmatrix} \mathcal{N}_{11}^{(j)} & \mathcal{N}_{12}^{(j)} \\ \mathcal{N}_{21}^{(j)} & \mathcal{N}_{22}^{(j)} \end{bmatrix} \begin{bmatrix} \partial_\nu u_{j-1}^+ \\ \partial_\nu u_j^- \end{bmatrix} = \begin{bmatrix} u_{j-1} \\ u_j \end{bmatrix}, \tag{17}$$

where $\mathcal{N}_j$ is given in 2×2 blocks. More precisely, the elimination process gives

$$\mathcal{N}_j = \begin{bmatrix} \mathcal{V}_{11}^{(j)} & \mathcal{V}_{14}^{(j)} \\ \mathcal{V}_{41}^{(j)} & \mathcal{V}_{44}^{(j)} \end{bmatrix} + \begin{bmatrix} \mathcal{C}_1\mathcal{D}_1 & \mathcal{C}_1\mathcal{D}_2 \\ \mathcal{C}_2\mathcal{D}_1 & \mathcal{C}_2\mathcal{D}_2 \end{bmatrix}, \tag{18}$$

where $\mathcal{C}_1$, $\mathcal{C}_2$, $\mathcal{D}_1$ and $\mathcal{D}_2$ are given by

$$\begin{aligned} &\mathcal{C}_1 = \mathcal{V}_{12}^{(j)} + \gamma\mathcal{V}_{13}^{(j)}, \quad \mathcal{C}_2 = \mathcal{V}_{42}^{(j)} + \gamma\mathcal{V}_{43}^{(j)}, \\ &\mathcal{D}_0 = \gamma\mathcal{V}_{22}^{(j)} + \gamma^2\mathcal{V}_{23}^{(j)} - \mathcal{V}_{32} - \gamma\mathcal{V}_{33}^{(j)}, \\ &\mathcal{D}_1 = \mathcal{D}_0^{-1}(\mathcal{V}_{31}^{(j)} - \gamma\mathcal{V}_{21}), \quad \mathcal{D}_2 = \mathcal{D}_0^{-1}(\mathcal{V}_{34}^{(j)} - \gamma\mathcal{V}_{24}^{(j)}). \end{aligned}$$

Using the definitions of $\mathcal{Q}_{j-1}^+$ and $\mathcal{Q}_j^-$ in (17), we obtain

$$\begin{aligned} (\mathcal{I} - \mathcal{N}_{11}\mathcal{Q}_{j-1}^+)u_{j-1} &= \mathcal{N}_{12}\mathcal{Q}_j^- u_j, \\ \mathcal{N}_{21}\mathcal{Q}_{j-1}^+ u_{j-1} &= (\mathcal{I} - \mathcal{N}_{22}\mathcal{Q}_j^-)u_j. \end{aligned}$$

To derive a formula for $\mathcal{Q}_j^-$, we solve u_{j-1} from the first equation above and insert it into the second equation. To find the formula for $\mathcal{Y}_j$, we use the definitions of $\mathcal{Y}_j$ and $\mathcal{Y}_{j-1}$ in the first equation. Therefore, the following marching formulae are obtained:

$$\mathcal{Z} = (\mathcal{I} - \mathcal{N}_{11}^{(j)}\mathcal{Q}_{j-1}^+)^{-1}\mathcal{N}_{12}^{(j)}, \tag{19}$$

$$Q_j^- = (\mathcal{N}_{22}^{(j)} + \mathcal{N}_{21}^{(j)}\mathcal{Q}_{j-1}^+\mathcal{Z})^{-1}, \tag{20}$$

$$\mathcal{Y}_j = \mathcal{Y}_{j-1}\mathcal{Z}\mathcal{Q}_j^-. \tag{21}$$

4. Boundary integral equations

In this section, we present the boundary integral equations that are used to calculate the NtD maps. Consider a domain Ω where the medium is homogeneous and the refractive index

$n = \sqrt{\varepsilon}$ is a constant, the Green's function of the Helmholtz equation (1) in such a medium is

$$G(\mathbf{r}, \tilde{\mathbf{r}}) = \frac{i}{4} H_0^{(1)}(k_0 n |\mathbf{r} - \tilde{\mathbf{r}}|), \tag{22}$$

where $\mathbf{r} = (x, y)$ and $\tilde{\mathbf{r}} = (\tilde{x}, \tilde{y})$, and G satisfies

$$\frac{\partial^2 G(\mathbf{r}, \tilde{\mathbf{r}})}{\partial x^2} + \frac{\partial^2 G(\mathbf{r}, \tilde{\mathbf{r}})}{\partial y^2} + k_0^2 n^2 G(\mathbf{r}, \tilde{\mathbf{r}}) = -\delta(\mathbf{r} - \tilde{\mathbf{r}}). \tag{23}$$

We denote the single- and double-layer integral operators $\mathcal{S}$ and $\mathcal{K}$ by

$$(\mathcal{S}\varphi)(\mathbf{r}) = 2 \int_{\partial\Omega} G(\mathbf{r}, \tilde{\mathbf{r}}) \varphi(\tilde{\mathbf{r}}) ds(\tilde{\mathbf{r}}), \quad \mathbf{r} \in \partial\Omega, \tag{24}$$

$$(\mathcal{K}\varphi)(\mathbf{r}) = 2 \int_{\partial\Omega} \frac{\partial G(\mathbf{r}, \tilde{\mathbf{r}})}{\partial \nu(\tilde{\mathbf{r}})} \varphi(\tilde{\mathbf{r}}) ds(\tilde{\mathbf{r}}), \quad \mathbf{r} \in \partial\Omega, \tag{25}$$

where φ is an arbitrary function defined on $\partial\Omega$.

If the boundary is smooth, then u and $\partial_\nu u$ satisfy the following boundary integral equation:

$$(1 + \mathcal{K})u = \mathcal{S} \frac{\partial u}{\partial \nu}. \tag{26}$$

Therefore, the NtD map for a smooth domain Ω is given by

$$\mathcal{V} = (1 + \mathcal{K})^{-1} \mathcal{S}.$$

If the boundary $\partial\Omega$ contains a corner at $\mathbf{r}_0$, we can use a boundary integral equation of the 2D Laplace equation to compensate the error appeared at the corner. Let $\mathcal{H}$ be the operator given by

$$(\mathcal{H}\varphi)(\mathbf{r}) = 2 \int_{\partial\Omega} \frac{\partial G_0(\mathbf{r}, \tilde{\mathbf{r}})}{\partial \nu(\tilde{\mathbf{r}})} \varphi(\tilde{\mathbf{r}}) ds(\tilde{\mathbf{r}}),$$

where

$$G_0(\mathbf{r}, \tilde{\mathbf{r}}) = \frac{1}{2\pi} \ln \frac{1}{|\mathbf{r} - \tilde{\mathbf{r}}|}, \quad \mathbf{r} \neq \tilde{\mathbf{r}},$$

then Eq. (26) should be modified as [33]:

$$(1 + \mathcal{K})u - u(\mathbf{r}_0)(1 + \mathcal{H}1) = \mathcal{S} \frac{\partial u}{\partial \nu}, \tag{27}$$

where $\mathcal{H}1$ means that the operator $\mathcal{H}$ is applied to the constant function 1 defined on $\partial\Omega$. If the boundary $\partial\Omega$ contains P corners at $\mathbf{r}_j$ for $1 \leq j \leq P$, we propose to use the following modified integral equation

$$(1 + \mathcal{K})u - v(\mathbf{r})(1 + \mathcal{H}1) = \mathcal{S} \frac{\partial u}{\partial \nu}, \tag{28}$$

where

$$v(\mathbf{r}) = \sum_{l=1}^{P} \prod_{j=1, j\neq l}^{P} \frac{|\mathbf{r} - \mathbf{r}_j|}{|\mathbf{r}_l - \mathbf{r}_j|} u(\mathbf{r}_l).$$

If $\partial_\nu u$ is given on $\partial\Omega$, we can use Eq. (28) to find u. Therefore, Eq. (28) allows us to find the NtD map $\mathcal{V}$, even when the boundary contains corners.

5. Nyström method with a graded mesh

To discretize the integral equation (28), we use the Nyström method with a graded mesh as in [33]. The discretization of the integral equation gives rise to the desired matrix approximations to the NtD map.

For a smooth boundary $\partial\Omega$, the Nyström method requires only a uniform mesh. The integral operators $\mathcal{S}$, $\mathcal{K}$ and $\mathcal{H}$ are discretized based on the following steps. First, we parametrize the boundary $\partial\Omega$ as a smooth 2π-periodic curve:

$$\mathbf{r}(t) = (x(t), y(t)), \quad 0 \le t \le 2\pi.$$

Any function defined on $\partial\Omega$ becomes a 2π-periodic function of t. For simplicity, we denote $\varphi(\mathbf{r})$ for $\mathbf{r} = \mathbf{r}(t) \in \partial\Omega$ by $\varphi(t)$. This applies to $\mathcal{S}\varphi$ and $\mathcal{K}\varphi$ in (24) and (25), since they are also functions defined on $\partial\Omega$. The operators $\mathcal{S}$, $\mathcal{K}$ and $\mathcal{H}$ are represented by bi-periodic kernels $S(t,\tau)$, $K(t,\tau)$ and $H(t,\tau)$. More specifically and for $\mathcal{S}$, we have

$$(\mathcal{S}\varphi)(t) = \int_0^{2\pi} S(t,\tau)\varphi(\tau)d\tau, \tag{29}$$

where τ is associated with $\tilde{\mathbf{r}}$ in (24) as $\tilde{\mathbf{r}} = (x(\tau), y(\tau))$. Next, we discretize t by a uniform mesh of J points: $t_j = 2\pi j/J$ for $0 \le j < J$, and approximate $(\mathcal{S}\varphi)(t_j)$ by quadrature schemes based on the same discretization points: $\tau_k = t_k$ for $0 \le k < J$. To obtain high accuracy in the numerical integrations, it is necessary to split the kernels S and K, such that

$$S(t,\tau) = S_1(t,\tau)\ln\left(4\sin^2\frac{t-\tau}{2}\right) + S_2(t,\tau). \tag{30}$$

where S_1, S_2, and the similarly defined K_1 and K_2 are smooth. For the smooth integrals associated with S_2, K_2 and H, the standard trapezoidal rule is used. For the parts with the logarithmic singularity, a special quadrature formula is available [33]. This gives rise to

$$(\mathcal{S}\varphi)(t_j) \approx \sum_{k=0}^{J-1} a_{jk}\varphi(t_k) \tag{31}$$

for some coefficients a_{jk}. With the similarly defined b_{jk} for operator $\mathcal{K}$, the integral equation (26) gives rise to the NtD map $\mathcal{V} \approx (I + A)^{-1}B$, where I is the identity matrix, A and B are $J \times J$ matrices with entries a_{jk} and b_{jk}.

For the case where the boundary has corners, we follow the graded mesh technique described in [33]. Starting from a parametric representation of the boundary: $\mathbf{r} = (x(t), y(t))$ for $0 \le t \le T$ (T does not need to be 2π), we assume that the P corners are

$$\mathbf{r}_l^* = (x(t_l^*), y(t_l^*)), \quad 0 \le l \le P,$$

where $t_0^* = 0$ and $t_P^* = T$ correspond to the same corner. A graded mesh on $\partial\Omega$ can be obtained if we introduce a new variable s (for $0 \le s \le 2\pi$) such that $t = w(s)$, and discretize

s uniformly. The corners are associated with s_l^* for $0 \le l \le P$ satisfying $t_l^* = w(s_l^*)$, where $s_0^* = 0$ and $s_P^* = 2\pi$ correspond to the same point. In the following, we discretize s uniformly by $s_j = 2\pi j/J$ for $0 \le j \le J$. The corners are assumed to be mesh points, that is, s_l^* for $0 \le l \le P$, are integer multiples of $2\pi/J$. For an integer $p \ge 2$, we define the function w on the interval (s_{l-1}^*, s_l^*), such that

$$\frac{d^k w}{ds^k} = 0 \quad \text{at} \quad s = s_{l-1}^*,\ s_l^* \quad \text{for} \quad k = 1, 2, ..., p-1. \tag{32}$$

$$\frac{dw}{ds} = 2\,\frac{t_l^* - t_{l-1}^*}{s_l^* - s_{l-1}^*} \quad \text{at} \quad s = \frac{s_{l-1}^* + s_l^*}{2}. \tag{33}$$

The first condition above indicates that the derivatives of w up to order $p-1$ must vanish at s_{j-1}^* and s_j^*. This allows us to have more points near the corners when s is uniformly sampled. The second condition (33) requires that the slope of w at the midpoint is twice the slope of the straight line connecting (s_{l-1}^*, t_{l-1}^*) and (s_l^*, t_l^*). This ensures that sampling points away from the corners are reasonably distributed. The function w is given by

$$w(s) = \frac{t_l^* w_1^p + t_{l-1}^* w_2^p}{w_1^p + w_2^p} \quad \text{for} \quad s_{l-1}^* \le s \le s_l^*, \tag{34}$$

where

$$w_1 = \left(\frac{1}{2} - \frac{1}{p}\right)\xi^3 + \frac{\xi}{p} + \frac{1}{2}, \quad w_2 = 1 - w_1, \quad \xi = \frac{2s - (s_{l-1}^* + s_l^*)}{s_l^* - s_{l-1}^*}.$$

With this change of variable, the boundary $\partial\Omega$ is now given using the parameter s:

$$\mathbf{r} = (x(w(s)), y(w(s))), \quad 0 \le s \le 2\pi.$$

The integral operators are discretized by the method described earlier with t replaced by s. At a corner, the normal derivative $\partial_\nu u$ is not uniquely defined. However, since $dw/ds = 0$ at the corners, the terms involving $\partial_\nu u$ at the corners vanish. In fact, the discretization of (28) gives rise to P equations for the corners, and they can be used to find u at the corners in terms of u and $\partial_\nu u$ at the other points. Therefore, we can eliminate u at the corners and obtain a NtD map which is approximated by a $(J-P)\times(J-P)$ matrix.

6. Least squares approach

In the first and last steps of the OM method, we need matrix approximations of the operators $\mathcal{B}^{(1)}$ and $\mathcal{B}^{(2)}$ to initialize $\mathcal{Q}_0^-$ and to solve the wave field at $y = D$. When the NtD maps of the sub-domains are calculated by the boundary integral equation method, we need a graded mesh to take care of the corners. Therefore, the line segments Γ_0 and Γ_m (at $y = 0$ and $y = D$, respectively) are discretized by a graded mesh. Since the mesh points near $x = 0$ or $x = L$ can be extremely close, it becomes numerically unstable to calculate matrix approximations of $\mathcal{B}^{(1)}$ and $\mathcal{B}^{(2)}$ directly based on these points.

To avoid this difficulty, we use a uniform mesh to approximate these operators and a least squares approach to relate two sets of mesh points. Let $\{x_k,\, 1 \le k \le N_1\}$ be the N_1 points of the graded mesh for discretizing $0 < x < L$. For a positive integer $N_2 < N_1$, we introduce a uniform mesh by

$$\xi_l = \frac{l - 0.5}{N_2} L, \quad l = 1, 2, ..., N_2.$$

Let f be a quasi-periodic function of x with N_2 Fourier modes, i.e.,

$$f(x) = \sum_j \hat{f}_j e^{i\alpha_j x},$$

where the index j is restricted to $-N_2/2 \le j < N_2/2$ or $|j| \le (N_2 - 1)/2$ for an even or odd N_2, respectively. For f evaluated at the graded and uniform mesh points, there is an $N_1 \times N_2$ matrix S, such that

$$\begin{bmatrix} f(x_1) \\ f(x_2) \\ f(x_3) \\ \vdots \\ f(x_{N_1}) \end{bmatrix} = S \begin{bmatrix} f(\xi_1) \\ f(\xi_2) \\ \vdots \\ f(\xi_{N_2}) \end{bmatrix}. \tag{35}$$

More precisely, we have $S = F_1 F_2^{-1}$, where F_1 and F_2 are matrices with entries $\exp(i\alpha_j x_k)$ and $\exp(i\alpha_j \xi_k)$, respectively. If f is a more general quasi-periodic function of x and if f is known at the graded mesh points $\{x_k\}$, we can calculate $f(\xi_k)$ for $1 \le k \le N_2$ in the least squares sense by

$$\begin{bmatrix} f(\xi_1) \\ f(\xi_2) \\ \vdots \\ f(\xi_{N_2}) \end{bmatrix} \approx S^\dagger \begin{bmatrix} f(x_1) \\ f(x_2) \\ f(x_3) \\ \vdots \\ f(x_{N_1}) \end{bmatrix}, \tag{36}$$

where $S^\dagger = (S^* S)^{-1} S^*$ is the pseudoinverse of S and S^* is the conjugate transpose of S.

The operators $\mathcal{B}^{(1)}$ and $\mathcal{B}^{(2)}$ can be approximated by $N_2 \times N_2$ matrices $\tilde{\mathcal{B}}^{(1)}$ and $\tilde{\mathcal{B}}^{(2)}$ satisfying

$$\tilde{\mathcal{B}}^{(s)} \phi_j = \beta_j^{(s)} \phi_j, \quad \phi_j = \begin{bmatrix} \exp(i\alpha_j \xi_1) \\ \exp(i\alpha_j \xi_2) \\ \vdots \\ \exp(i\alpha_j \xi_{N_2}) \end{bmatrix} \tag{37}$$

for j restricted to N_2 different values as before. Therefore,

$$\tilde{\mathcal{B}}^{(s)} = \tilde{\mathcal{P}} \tilde{\mathcal{D}}^{(s)} \tilde{\mathcal{P}}^{-1}, \tag{38}$$

where $\tilde{\mathcal{P}}$ is the matrix with columns ϕ_j, and $\tilde{\mathcal{D}}^{(s)}$ is a diagonal matrix with diagonal entries $\beta_j^{(s)}$. To initialize $\mathcal{Q}_0^-$, we need an $N_1 \times N_1$ matrix for $\mathcal{B}^{(2)}$ corresponding to the graded mesh. This can be obtained by

$$\mathcal{B}^{(2)} = S\tilde{\mathcal{B}}^{(2)}S^\dagger. \tag{39}$$

For the last step, we can transform the $N_1 \times N_1$ matrix $\mathcal{Q}_m^+$ for the graded mesh to an $N_2 \times N_2$ matrix $\tilde{\mathcal{Q}}_m^+$ for the uniform mesh, then solve u on the uniform mesh using $\tilde{\mathcal{B}}^{(1)}$ directly. The formula for $\tilde{\mathcal{Q}}_m^+$ is

$$\tilde{\mathcal{Q}}_m^+ = S^\dagger \mathcal{Q}_m^+ S. \tag{40}$$

Similarly, we transform the $N_1 \times N_1$ matrix $\mathcal{Y}_m$ for the graded mesh to an $N_2 \times N_2$ matrix $\tilde{\mathcal{Y}}_m$, then calculate the transmitted field for the uniform mesh.

7. Numerical examples

In this section, we illustrate our method by a few examples and compare our results with those published by other authors. The first example is a dielectric sinusoidal grating as shown in Fig. 3(a). The interface is a sine function with period L and magnitude $d/2$, and

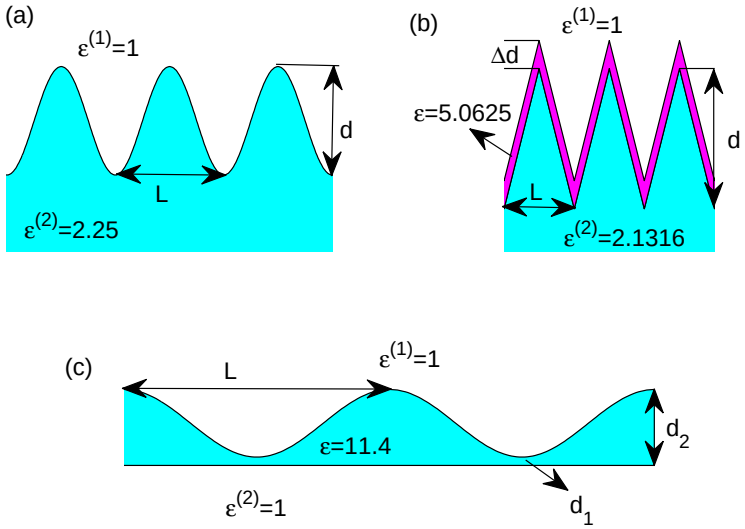

Fig. 3. (a) A sinusoidal grating with a dielectric substrate; (b) a triangular grating with high-index coating layer; (c) a sinusoidal grating with a free space bottom.

it separates air and a homogeneous dielectric medium. Following the early work of Li [6],

we assume that the dielectric constant of the medium below the interface is $\varepsilon = 2.25$, the groove depth is $d = L$, the free space wavelength of the incident wave is $\lambda = L/1.7$, and the angle of incidence (between the y axis and the wave vector) is $\pi/6$. Therefore, the wave vector of the incident wave is $(\alpha_0, -\beta_0^{(1)}) = (k_0/2, -\sqrt{3}k_0/2)$. In Table 1, we show the first a

Table 1. Comparison of diffraction efficiencies for a sinusoidal grating.

Polarization	Order	Li (C method)	This work
TE	R, -1	0.7815037×10^{-3}	0.78150378×10^{-3}
TE	R, 0	0.2103160×10^{-2}	0.21031606×10^{-2}
TE	T, -1	0.4947933	0.49479330
TE	T, 0	0.2086662	0.20866625
TE	T, 1	0.1183058	0.11830582
TM	R, -1	0.6922409×10^{-3}	0.69224074×10^{-3}
TM	R, 0	0.1908596×10^{-3}	0.19085979×10^{-3}
TM	T, -1	0.4612936	0.46129364
TM	T, 0	0.1845351	0.18453510
TM	T, 1	0.1256906	0.12569059

few transmitted and reflected diffraction efficiencies for both TE and TM polarizations. For comparison, we also list the diffraction efficiencies calculated by Li using the C method [22]. We can see that the results obtained using the two different methods are nearly identical. This is true even for the relatively small reflected diffraction efficiencies. To obtain the results in Table 1, we choose a rectangular domain Σ with its lower and upper edges strictly below and above the interface. Each of the two homogeneous sub-domains of Σ has four corners. The NtD maps for these two sub-domains are calculated by discretizing the boundary of these sub-domains using $J = 320$ points. For the graded mesh, we use the parameter $p = 5$. On the top and bottom edges Γ_0 and Γ_2, we have $N_1 = 39$ and $N_2 = 15$ points for the graded mesh and the uniform mesh, respectively.

The second example, as shown in Fig. 3(b), is a triangular grating with a coating layer. It is designed as a guided-mode resonant grating filter and it was previously analyzed by Mizutani *et al* [34]. The dielectric constant of the substrate and the thin film are $\varepsilon^{(2)} = 2.1316$ and $\varepsilon = 5.0625$, respectively. The medium above the grating structure is air. The height of the triangular region of the substrate is $d = 2L$, where L is the period in the x direction. The high-index coating layer has a vertical thickness of Δd as shown in Fig. 3(b). We consider two cases for $\Delta d = 0.4L$ and $\Delta d = L$, respectively. For normal incident wave, the results are shown in Fig. 4. Our results agree with those reported in [34]. For this problem, we choose a rectangular domain Σ that contains three sub-domains Ω_1, Ω_2 and Ω_3. These three sub-

domains correspond to the substrate, thin film and air, respectively. The results shown in Fig. 4 are obtained using a graded mesh with $p = 8$. The boundaries of the three sub-domains

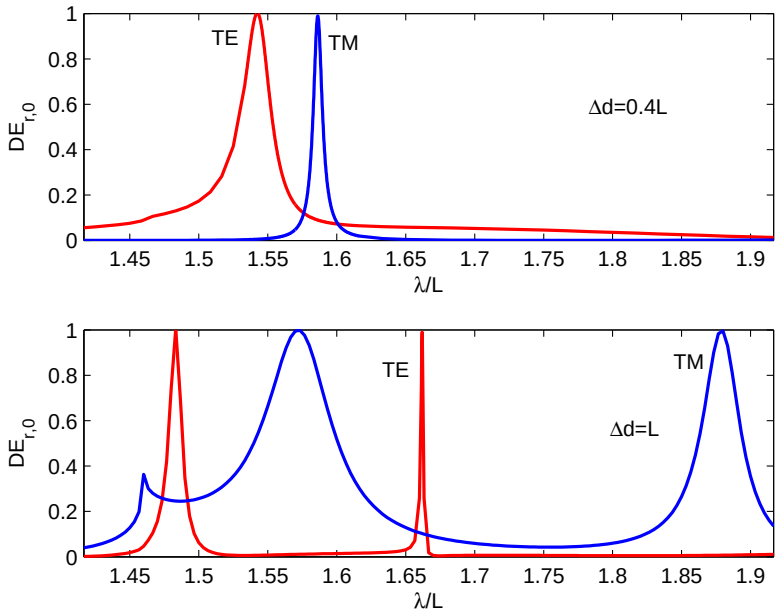

Fig. 4. Zeroth order reflected diffraction efficiencies of a coated triangular grating as functions of the wavelength.

are discretized by $J = 480$ points, respectively. On the top and bottom line segments Γ_0 and Γ_3, we have $N_1 = 39$ points in the graded mesh and $N_2 = 15$ points in the uniform mesh.

The third example is also a sinusoidal grating. However, the structure is finite in the y direction. As shown in Fig. 3(c), the dielectric grating is bounded by a sinusoidal interface on the top and a flat interface at the bottom. The medium above and below the grating structure is air. Using the notations of Section 2, we have $\varepsilon^{(1)} = \varepsilon^{(2)} = 1$. This example was previously analyzed by Magath *et al* [18] by an integral equation method. As in [18], we assume that the dielectric constant of the grating medium is $\varepsilon = 11.4$, and the sinusoidal interface has a period L and a magnitude $0.4L/\pi$. The lower interface is located at $d_1 = 0.1L/\pi$ below the lowest points of the sinusoidal interface. As a result, the structure has a minimum thickness of d_1 and a maximum thickness of $d_2 = 0.9L/\pi$. In Table 2, we show the diffraction efficiencies for the TE polarization and for two difference wavelengths. The angle of incidence is 15.2575° and 30° for $L/\lambda = 1.9$ and $L/\lambda = 1$, respectively. The results of Magath *et al* [18] are also listed for comparison. We can see that the agreement is quite good, since the first three digits of all diffraction efficiencies are identical. Our results are obtained by choosing the rectangular domain Σ, such that its lower edge Γ_0 coincides with the lower interface. Meanwhile, Σ consists of two homogeneous sub-domains separated Γ_1 which coincides with

Table 2. Comparison of diffraction efficiencies for a sinusoidal grating with free space bottom.

L/λ	Order	Magath [18]	This work
1.9	R, -2	0.1632	0.16337787
1.9	R, -1	0.5312	0.53111858
1.9	R, 0	0.0650	0.06506795
1.9	R, 1	0.1538	0.15381827
1	R, -1	0.0401	0.03989897
1	R, 0	0.4777	0.47833249
1	T, -1	0.2794	0.27947198
1	T, 0	0.2029	0.20229650

the sinusoidal interface. In our calculations, the boundaries of the two sub-domains Ω_1 and Ω_2 are discretized by $J = 360$ points. The parameter for generating the graded mesh is $p = 5$. On the top and bottom edges Γ_2 and Γ_0, we have $N_1 = 119$ and $N_2 = 25$ points in the graded mesh and the uniform mesh, respectively.

For the above examples, we performed additional calculations using different values of p and J. The integer p is used to tune the density of points near the corners for the graded mesh. In principle, a larger p gives a higher order of accuracy. In practice, if the required accuracy is not very high, many different values of p, say $2 \leq p \leq 9$, all work quite well. For each sub-domain Ω_j, the integer J depends on the total length of the boundary $\partial\Omega_j$, the number of corners, the wavelength for the homogeneous medium in Ω_j and the value of p. When J is increased, we can observe fast numerical convergences of the diffraction efficiencies. The integer N_2 is chosen such that the grid size of the uniform mesh (on the line segments Γ_0 and Γ_m) is always larger than the maximum distance between two nearby points of the graded mesh.

8. Conclusions

In this paper, we developed a new method for analyzing diffraction gratings based on boundary integral equations and Neumann-to-Dirichlet maps. Existing boundary integral equation methods for diffraction gratings are powerful methods that can give accurate results, but they are somewhat complicated to implement, since the kernels of the integral operators are related to the quasi-periodic Green's function which is difficult to evaluate. Our method divides a period of the grating structure into homogeneous sub-domains, then uses boundary integral equations to calculate the NtD maps of these sub-domains. The integral operators appeared in our method are derived from the standard Green's function of the Helmholtz

equation in a homogeneous medium, and they are much easier to discretize. Although our method is very different from existing boundary integral equation methods, it seems to retain all their advantages. Numerical examples indicate that high accuracy can be achieved when relatively small number of points are used to discretize the boundaries of the homogeneous sub-domains.

Acknowledgments

The authors sincerely thank Professor Lifeng Li of Tsinghua University for analyzing the sinusoidal grating by the C method, providing the results to us for comparison (in Table 1) and giving us valuable references. This research was partially supported by a grant from the Research Grants Council of Hong Kong Special Administrative Region, China (Project No. CityU 102008).

References

1. R. Petit, ed., Electromagnetic Theory of Gratings (Speinger-Verlag, Berlin, 1980).
2. G. Bao, L. Cowsar, and W. Masters, ed., Mathematical Modeling in Optical Sciences (Society for Industrial and Applied Mathematics, 2001).
3. M. Nevière and E. Popov, Light Propagation in Periodic Media, Marcel Dekker, Inc. 2003.
4. L. C. Botten, M. S. Craig, R. C. McPhedran, J. L. Adams, and J. R. Andrewartha, "The dielectric lamellar diffraction grating," Optica Acta **28**, 413-428 (1981).
5. L. C. Botten, M. S. Craig, R. C. McPhedran, J. L. Adams, and J. R. Andrewartha, "The finitely conducting lamellar diffraction grating," Optica Acta **28**, 1087-1102 (1981).
6. L. Li, "Multilayer modal method for diffration gratings of arbitrary profile, depth, and permittivity," J. Opt. Soc. Am. A **10**, 2581-2591 (1993).
7. M. G. Moharam and T. K. Gaylord, "Diffraction analysis of dielectric surface-relief gratings," J. Opt. Soc. Am. **72**, 1385-1392 (1982).
8. P. Lalanne and G. M. Morris, "Highly improved convergence of the coupled-wave method for TM polarization," J. Opt. Soc. Am. A **13**, 779-784 (1996).
9. G. Granet and B. Guizal, "Efficient implementation of the coupled-wave method for metallic lamellar gratings in TM polarization," J. Opt. Soc. Am. A **13**, 1019-1023 (1996).
10. L. Li, "Use of Fourier series in the analysis of discontinuous periodic structures," J. Opt. Soc. Am. A **13**, 1870-1876 (1996).
11. E. Popov and M. Nevière, "Grating theory: new equations in Fourier space leading to fast converging results for TM polarization," J. Opt. Soc. Am. A **17**, 1773-1784 (2000).

12. E. Popov and M. Nevière, "Maxwell equations in Fourier space: A fast-converging formulation for diffraction by arbitrary shaped, periodic, anisotropic media," J. Opt. Soc. Am. A **18**, 2886-2894 (2001).
13. D. Maystre, "Integral Methods," in *Electromagnetic Theory of Gratings*, R. Petit, ed. (Speinger-Verlag, Berlin, 1980), Chapter 3.
14. A. Pomp, "The integral method for coated gratings – computational cost," J. Mod. Opt. **38**, 109-120 (1991).
15. B. H. Kleemann, A. Mitreiter, and F. Wyrowski, "Integral equation method with parametrization of grating profile - Theory and experiments," J. Mod. Opt. **43**, 1323-1349 (1996).
16. D. W. Prather, M. S. Mirotznik, and J. N. Mait, "Boundary integral methods applied to the analysis of diffractive optical elements," J. Opt. Soc. Am. A **14**, 34-43 (1997).
17. E. Popov, B. Bozhkov, D. Maystre, and J. Hoose, "Integral method for echelles covered with lossless or absorbing thin dielectric layers," Appl. Opt. **38**, 47-55 (1999).
18. T. Magath and A. E. Serebryannikov, "Fast iterative, coupled-integral-equation technique for inhomogeneous profiled and periodic slabs," J. Opt. Soc. Am. A **22**, 2405-2418 (2005).
19. A. Rathsfeld, G. Schmidt, and B. H. Kleemann, "On a fast integral equation method for diffraction gratings," Commun. Comput. Phys. **1**, 984-1009 (2006).
20. J. Chandezon, D. Maystre, and G. Raoult, "A new theoretical method for diffraction gratings and its numerical application," Journal of Optics **11**, 235-241 (1980).
21. J. Chandezon, M. T. Dupuis, G. Cornet, and D. Maystre, "Multicoated gratings – a differential formalism applicable in the entire optical region," J. Opt. Soc. Am. **72**, 839-846 (1982).
22. L. Li, J. Chandezon, G. Granet, and J. P. Plumey, "Rigorous and efficient grating-analysis method made easy for optical engineers," Appl. Opt. **38**, 304-313 (1999).
23. G. Bao, Z. M. Chen, and H. J. Wu, "Adaptive finite-element method for diffraction gratings," J. Opt. Soc. Am. A **22**, 1106-1114 (2005).
24. E. Popov, M. Nevière, B. Gralak, and G. Tayeb, "Staircase approximation validity for arbitrary-shaped gratings," J. Opt. Soc. Am. A **19**, 33-42 (2002).
25. Y. Huang and Y. Y. Lu, "Scattering from periodic arrays of cylinders by Dirichlet-to-Neumann maps," J. Lightwave Technol. **24**, 3448-3453 (2006).
26. Y. Huang and Y. Y. Lu, "Modeling photonic crystals with complex unit cells by Dirichlet-to-Neumann maps," J. Comput. Math. **25**, 337-349 (2007).
27. Y. Wu and Y. Y. Lu, "Dirichlet-to-Neumann map method for analyzing interpenetrating cylinder arrays in a triangular lattice," J. Opt. Soc. Am. B **25**, 1466-1473 (2008).
28. Y. Wu and Y. Y. Lu, "Dirichlet-to-Neumann map method for analyzing periodic arrays

of cylinders with oblique incident waves," J. Opt. Soc. Am. B **26**, 1442-1449 (2009).
29. R. C. McPhedran, L. C. Botten, A. A. Asatryan, N. A. Nicorovici, P. A. Robinson, and C. M. de Sterke, "Calculation of electromagnetic properties of regular and random arrays of metallic and dielectric cylinders," Phys. Rev. E **60**, 7614-7617 (1999).
30. K. Yasumoto, H. Toyama, and T. Kushta, "Accurate analysis of two-dimensional electromagnetic scattering from multilayered periodic arrays of circular cylinders using lattice sums technique," IEEE Transactions on Antennas and Propagation **52**, 2603-2611 (2004).
31. G. Bao, D. C. Dobson and J. A. Cox, "Mathematical studies in rigorous grating theory," J. Opt. Soc. Am. A **12**, 1029-1042 (1995).
32. Y. Y. Lu and J. R. McLaughlin, "The Riccati method for the Helmholtz equation," J. Acoust. Soc. Am. **100**, 1432-1446 (1996).
33. D. Colton and R. Kress, *Inverse Acoustic and Electromagnetic Scattering Theory*, 2nd ed. (Springer-Verlag, Berlin, 1998).
34. A. Mizutani, H. Kikuta, K. Iwata, and H. Toyota, "Guided-mode resonant grating filter with an antireflection structure surface," J. Opt. Soc. Am. A **19**, 1346-1351 (2002).